Layout optimization and performance analysis of large array of imaging atmospheric Cherenkov telescopes*

Zhipeng Zhang (张志鹏)[1] Ruizhi Yang (杨睿智)[1,2,3,6†] Shoushan Zhang (张寿山)[4,5,6] Zhen Xie (谢禛)[1]
Jiali Liu (刘加丽)[4,5,6] Liqiao Yin (尹丽巧)[4,5,6] Yudong Wang (王玉东)[4,5,6]
Lingling Ma (马玲玲)[4,5,6] Zhen Cao (曹臻)[4,5,6]

[1]School of Astronomy and Space Science, University of Science and Technology of China, Hefei 230026, China
[2]CAS Key Laboratory for Research in Galaxies and Cosmology, Department of Astronomy, University of Science and Technology of China, Hefei 230026, China
[3]Deep Space Exploration Laboratory/School of Physical Sciences, University of Science and Technology of China, Hefei 230026, China
[4]Key Laboratory of Particle Astrophysics, Institute of High Energy Physics, Beijing 100049, China
[5]Department of Physics, University of Chinese Academy of Sciences, Beijing 100049, China
[6]Tianfu Cosmic Ray Research Center, Chengdu 610299, China

Abstract: The large array of imaging atmospheric Cherenkov telescopes (LACT) is a planned array of 32 Cherenkov telescopes, each featuring 6-m diameter mirrors, to be constructed at the LHAASO site. This study focused on optimizing the array layout and analyzing the performance of LACT. Two observation modes were examined: large zenith angle observations for ultra-high energy events and small zenith angle observations for lower energy thresholds. For large zenith angles (60°), simulations indicate that an 8-telescope subarray can achieve an effective area of 3 km^2 with excellent angular resolution. For small zenith angles, we optimized the layout of 4-telescope cells and the full 32-telescope array. The energy threshold of the full array is approximately 200 GeV, which is particularly crucial for studying transient phenomena such as gamma-ray bursts (GRBs) and active galactic nuclei (AGNs). This study provides essential guidance for finalizing the LACT layout design and estimating performance under various observational conditions. It also highlights the potential of LACT for conducting deep observations of ultra-high energy γ-ray sources, performing morphological studies of PeVatrons, and advancing time-domain γ-ray astronomy.

Keywords: IACT, γ-ray, LHAASO

DOI: 10.1088/1674-1137/ad8e3f **CSTR:** 32044.14.ChinesePhysicsC.49035001

I. INTRODUCTION

The field of ground-based γ-ray astronomy has evolved significantly since its inception in the mid-20th century. Because the Earth's atmosphere is opaque to γ-rays, this field relies on detecting secondary particles produced when γ-rays interact with the atmosphere. Two primary types of detectors have driven this evolution: imaging atmospheric Cherenkov telescopes (IACTs) and extensive air shower (EAS) arrays. IACTs, such as those developed at the Whipple Observatory in the 1960s [1], detect γ-rays by capturing the Cherenkov light emitted by charged secondary particles resulting from γ-ray interactions in the atmosphere. This technique enables high-resolution imaging of γ-ray sources. In contrast, EAS arrays, including the Tibet AS-γ [2] and ARGO-YBJ [3], directly detect secondary particles that reach the ground. These arrays provide a broad field of view and are particularly well-suited for surveying large portions of the sky.

Over the past 20 years, IACTs have played a pivotal role in advancing the field of TeV γ-ray astronomy. The current generation of IACTs, including H.E.S.S. [4], VERITAS [5], and MAGIC [6] has made numerous significant contributions, substantially enriching our understanding of high-energy phenomena in the universe. To date, more than 300 TeV sources have been detected, the majority of which are credited to IACTs[1)].

The landscape of γ-ray astronomy is increasingly be-

Received 23 September 2024; Accepted 4 November 2024; Published online 5 November 2024

* Rui-zhi Yang is supported by the National Nature Science Foundation of China (12041305), the National Youth Thousand Talents Program in China, and the Sichuan Science and Technology Department, Institute of High Energy Physics (2023YFSY0014, E25156U1). This study was also supported by the Sichuan Province Science Foundation for Distin-guished Young Scholars (2022JDJQ0043), the Sichuan Science and Technology Department (2023YFSY0014), the Xiejialin Foundation of IHEP (E2546IU2), the National Natural Science Foundation of China (12261141691), and the Innovation Project of IHEP (E25451U2)

† E-mail: yangrz@ustc.edu.cn

1) http://tevcat.uchicago.edu/

ing shaped by the Large High Altitude Air Shower Observatory (LHAASO) [7]). As a leading facility in EAS arrays, LHAASO has pioneered ultra-high energy (UHE) γ-ray astronomy with unprecedented sensitivity above 20 TeV. It opened new frontiers in the field by detecting the first 12 UHE γ-ray sources in the Galactic plane [8].

LHAASO has recently published its first catalog (1LHAASO [9]), which includes over 90 high-energy γ-ray sources. Notably, 43 of these sources have energies exceeding 100 TeV. These sources are considered candidates for PeV particle accelerators, known as PeVatrons, and are crucial for understanding the origin of cosmic rays (CRs) in our Galaxy. However, most of these sources are spatially extended, and the limited angular resolution of LHAASO poses challenges for the determination of the origins of these UHE γ-ray emissions [10]. While IACT arrays offer superior angular resolution, the effective area of current IACT arrays is approximately 10^5 m^2, limiting their ability to have good synergy with LHAASO. The next generation of Cherenkov telescope arrays, such as the Cherenkov Telescope Array (CTA) [11]) and ASTRI [12], will feature effective areas exceeding 10^6 m^2. With their enhanced angular resolution and larger effective areas, these arrays will provide a powerful complement to LHAASO. Additionally, we propose the Large Array of Imaging Atmospheric Cherenkov Telescopes (LACT) [13]) at the LHAASO site as a crucial advancement in this direction. LACT will provide significantly improved sensitivity and angular resolution, enabling detailed studies of LHAASO-detected sources, particularly in the ultra-high energy range.

Previous studies have explored various array designs optimized for the detection of ultra-high-energy γ-rays above 10 TeV. Plyasheshnikov *et al.* [14] demonstrated that an IACT cell with modest mirror size, a wide field of view, and large spacing could deliver excellent performance. This cell-based concept was further developed by the TenTen project [15], which proposed an array composed of multiple such cells to achieve effective areas exceeding 10 km2. These pioneering efforts provide valuable guidance for the design of LACT.

LACT comprises 32 telescopes, each featuring a 6 m diameter. These telescopes leverage SiPM technology for their cameras, a technology which has been already validated on WFCTA [16]. This advancement will allow the telescopes to operate during moon nights, significantly increasing the observation time. The primary scientific objective of LACT is to conduct long-term observations of PeVatron candidates detected by LHAASO, leveraging its superior angular resolution to study the morphology of these sources. Additionally, LACT is designed to perform effectively at energies below 1 TeV, enabling the observation of extragalactic sources and γ-ray transients detected by LHAASO-WCDA [17]. This capability greatly broadens the scientific scope of LACT. To address these goals, two observation modes are proposed: one focusing on large zenith angle observations for ultra-high energy events and the other employing normal small zenith angle observations. Optimizing the layout of LACT must account for the requirements of both modes. Given the complexity of telescope configurations and the need to evaluate baseline performance for both observation strategies, this study was conducted to guide the final array layouts and estimate the performance of LACT under various observational conditions.

This paper is organized as follows. Section II provides a brief introduction to the Monte Carlo simulation and reconstruction methods. Section III examines the layout and performance of the array for large zenith angle observations. Section IV focuses on the small zenith angle observations, starting with the performance of an individual cell and then analyzing the full array. Finally, Section V presents our conclusions and discusses the implications of the results.

II. SIMULATION AND RECONSTRUCTION METHODS

We used the CORSIKA [18] package (version 7.64) to produce γ-rays and proton air showers. For electromagnetic interactions, we employed the EGS4 model, while for hadronic interactions, we used the URQMD model at low energies and the QGSJET-II model at high energies. The photon files obtained from CORSIKA were used as input for sim_telarray [19] to generate the response of the telescope. The telescope configuration used in the simulation features a Davies-Cotton mirror design with a 6 m diameter and an 8 m focal length. The camera of the telescope consists of over 1400 pixels, each measuring 25.8 mm, providing a total field of view of 8° in diameter. In this simulation, events were generated for point-like γ-rays, diffuse γ-rays, and diffuse protons at zenith angles of 20° and 60°. The diffuse gamma rays and diffuse protons were randomly distributed within a cone of 7° radius centered on the simulated point-like source. To increase the number of showers, shower events were reused: point-like gamma events were reused 10 times, while diffuse gamma and diffuse proton events were reused 20 times each. The night sky background (NSB) was modeled using real measurements from LHAASO-WFCTA, corresponding to an NSB rate of approximately 0.1 pe m^{-2}ns^{-1}deg^{-2}. Considering the mirror area and pixel size of the LACT telescope, we modeled a Poisson distribution with a mean of 7 p.e.. Note that the electronics and atmospheric profile used in this simulation do not fully represent real conditions of LACT, and more detailed modeling is needed. The parameters employed in the simulation are provided in Table 1.

For each event, we required at least two telescopes to trigger. We first performed image cleaning on the tele-

Table 1. Simulation parameters.

Particle type	Index	Energy range /TeV	View cone radius /deg	Scatter radius /m	Azimuth direction /deg	Zenith angle/deg	Number of shower
gamma (point-like)	–2	0.4–400	0	1800	0	60	10^8
gamma (diffuse)	–2	0.4–400	7	2000	0	60	6×10^8
proton	-2	0.6–600	7	2000	0	60	1.8×10^9
gamma (point-like)	–2	0.1–400	0	1600	0	20	4×10^8
gamma (diffuse)	–2	0.1–400	7	1800	0	20	1.5×10^9
proton (diffuse)	–2	0.1–600	7	1800	0	20	4×10^9

scope images using a two-level tail-cut method. This method requires a pixel to exceed a specified high threshold, with at least one neighboring pixel exceeding a lower threshold, or vice versa [20]. After image cleaning, the image was parameterized [21]. In addition to the standard Hillas parameters, we introduced the MISS parameter, which is defined as the distance from the true source position to the major axis in the nominal plane. The MISS parameter serves as an indicator of the reconstruction accuracy of the shower-detector plane (SDP) for a single telescope, and we will frequently refer to it in the following sections. For reconstruction, we required at least two telescopes to meet the following selection criteria: SIZE > 100 photoelectrons (p.e.) and LEAKAGE2 < 0.3, where SIZE represents the total p.e. in the image after cleaning, and LEAKAGE2 is the ratio of p.e. in the outermost two layers of pixels. It is important to note that these selection cut conditions have not been fully optimized and are only preliminary. The direction of the incoming shower was reconstructed by the intersection of the major axes in the reference telescope frame. After reconstructing the direction and core position of each event, we calculated the corresponding reconstructed impact parameter. Combining this with the parameters obtained from the telescopes, we trained a Random-Forest-Regressor model for energy reconstruction and a Random-ForestClassifier model for particle separation [22] using diffuse gamma events and diffuse proton events. The estimated energy and hadronness of a single telescope were combined with weights to determine the overall reconstructed energy and hadronness of the event. For easier comparison, we present the angular resolution and collection area after event selection in relation to the true energy in the following sections.

III. LARGE ZENITH ANGLE OBSERVATION

The technique of increasing the effective area of Cherenkov telescopes at high energies by observing at large zenith angles (LZA) was proposed early on [23] and systematically investigated in [24]. This approach has been widely applied to existing IACTs: MAGIC, by using the Very Large Zenith Angle observation mode (zenith angles of 70°–80°), increased the collection area to 2 km^2 and successfully detected the spectrum of the Crab Nebula up to 100 TeV [25]. In addition to expanding the effective area, observations at LZA also enhance the sky coverage of IACTs. VERITAS has studied the Galactic Center region, which can only be observed using LZA at the VERITAS site [26]. Similarly, for LACT, during the appropriate observation period, the Galactic Center (RA: 17 h 45 m 39.6 s, DEC: –29° 00' 22") can only be observed at zenith angles greater than 50°.

Compared to existing IACTs, which are typically located at altitudes around 2000 m, the LHAASO site, at a higher altitude of 4400 m, benefits even more from the advantages of LZA observations. At the LHAASO site, the shower maximum for 100 TeV gamma-ray showers is very close to the ground, resulting in a steep photon lateral distribution, which can cause significant image leakage in the telescopes. However, in the LZA observation mode, the increased atmospheric depth between the shower maximum and the telescope flattens the lateral distribution of photons, leading to smaller and higher-quality images. In Fig. 1, we show the relationships between the observed SIZE and impact parameter, as well as LEAKAGE2 and impact parameter, for γ-ray showers around 100 TeV at zenith angles of 20° and 60°. Figure 1(a) shows that at a zenith angle of 60°, the image of the telescope still contains a significant number of p.e. even with an impact parameter greater than 800 m. In contrast, at smaller zenith angles, the steeper lateral distribution limits the detectable distance of the telescope. Considering the cuts used in our analysis, i.e., SIZE > 100 p.e. and LEAKAGE2 < 0.3, the detectable distance of a single telescope extends from 300 m in the low zenith mode to over 800 m in the LZA mode. This significant increase in the detectable distance increases both the collection area and the multiplicity of events.

Although the LZA mode can significantly increase the effective area, the angular resolution at LZA for existing IACTs is worse (> 0.1°). This limitation arises because the distance between telescopes in current IACT arrays is approximately 100 m. When observing distant events at large zenith angles, the images captured by different telescopes are nearly parallel, making effective stereoscopic reconstruction difficult [27]. Based on the con-

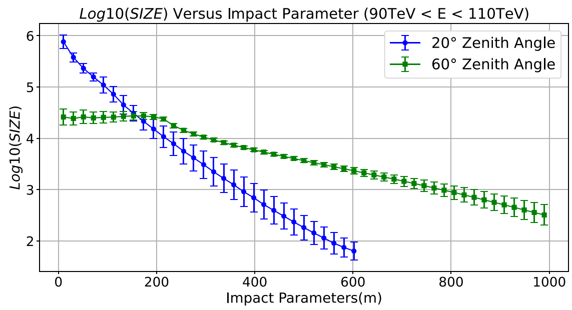

(a) The total number of photoelectrons in the telescope after image clean versus the impact parameter.

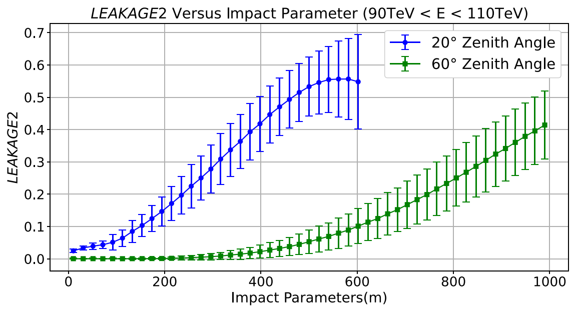

(b) *LEAKAGE2* versus impact parameter.

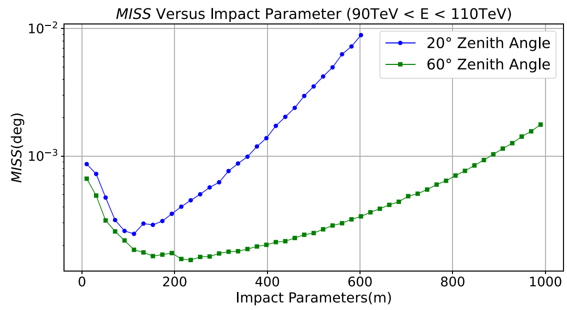

(c) Mean *MISS* versus impact parameter.

Fig. 1. (color online) Comparison of some parameters for small (20°) and large (60°) zenith angles.

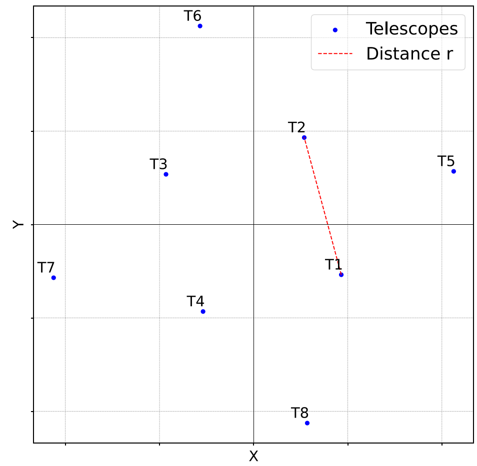

Fig. 2. (color online) Telescope layout for eight telescopes. The line between Tel.1 and Tel.2 represents the distance r.

siderations above, we propose dividing the 32 telescopes of LACT into four groups for LZA observations, with each group consisting of eight well-separated telescopes. To ensure similar performance across all groups, we first divided the 32 telescopes into 8 cells, each containing four closely spaced telescopes. Under LZA observations, the eight telescopes from different cells can be combined to form four groups. This arrangement ensures that each group maintains optimal performance in the LZA mode. To further explore whether increasing the distance between telescopes improves performance at large zenith angles, we conducted the following studies. Figure 2 shows the layout of eight telescopes, where r represents the distance between each telescope and its nearest neighbor. In the simulation, we considered scenarios with r values of 300, 400, and 500 m, respectively. The simulated γ-ray showers have a zenith angle of 60° and an energy range from 400 GeV to 400 TeV.

A. Comparison of different layouts

The angular resolution and collection area for different distances are shown in Fig. 3 and Fig. 4. As expected, above several TeV, the overall performance improves with increasing distance, both in terms of collection area and angular resolution. Considering that the detectable distance of a single telescope (> 800 m) is much greater than the distance between telescopes, extending the distance from 300 to 500 m allows for coverage of a larger area, thereby increasing the collection area. Additionally, as most events occur outside the array, increasing the distance between telescopes improves stereoscopic reconstruction, thereby enhancing angular resolution. We found that the collection area reaches its maximum at approximately 30 TeV. Below 30 TeV, the LEAKAGE2 cut is less restrictive, resulting in a larger collection area but poorer angular resolution. As the energy increases, the LEAKAGE2 cut becomes more effective, causing the collection area to gradually decrease with increasing energy. Notably, at LZA, the performance at high energies shows significant improvement compared to smaller zenith angles. In former studies [28], we investigated the performance of similar eight telescope configurations at 20° zenith angle. The results showed that at LZA, the collection area increases threefold (from 1 km^2 to 3 km^2), accompanied by a substantial improvement in angular resolution, especially in the energy range above 100 TeV. This enhanced performance at LZA can be attributed to the significantly higher altitude of LACT. At lower zenith angles, the image of the air shower in the camera is much larger, resulting in significant image leakage even with the larger 8° field of view. This leads to poorer image quality at high energies and reduced collection area after

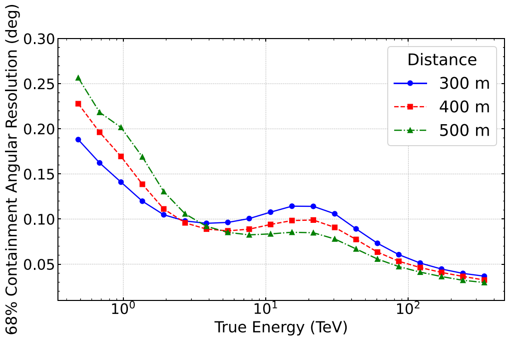

Fig. 3. (color online) Angular resolution after event preselection at large zenith angle for different distances.

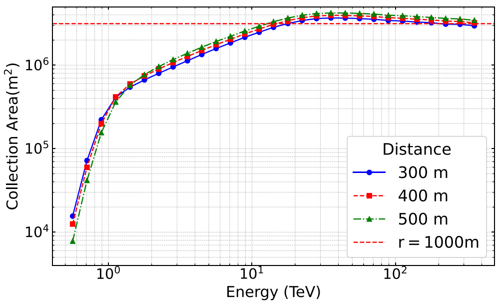

Fig. 4. (color online) Collection area after event preselection at large zenith angle for different distances. The red dashed line represents the area corresponding to a circle with a radius of 1000 m.

event selection. In contrast, in LZA mode, the smaller images from more distant air showers result in better image quality and more accurate direction reconstruction from individual telescopes, compensating for the less effective stereoscopic reconstruction. Figure 1(c) shows the relationship between the average *MISS* and the impact parameter. Owing to the smaller physical size of the images at LZA, the corresponding *MISS* is much smaller. Even at an impact parameter of 600 m, the SDP accuracy obtained from the telescope is approximately 0.03°, enabling very precise direction reconstructions. Considering the actual geographic conditions, the distance between different cells should be within the range of 360 to 410 m. Therefore, we will use 400 m as the basis for the following discussion.

B. Offset performance at LZA

Owing to the use of the Davies-Cotton single mirror design, the optical performance of the LACT telescope degrades significantly with offset compared to ASTRI [29] and CTA-SST, which use a dual mirror design. As a result, unlike ASTRI, which maintains a relatively uniform angular resolution within at least 3° off-axis [12], the angular resolution of LACT deteriorates more significantly as the off-axis angle increases. However, at LZA, the image size becomes smaller, which helps reduce the degradation in off-axis observations. This makes LZA

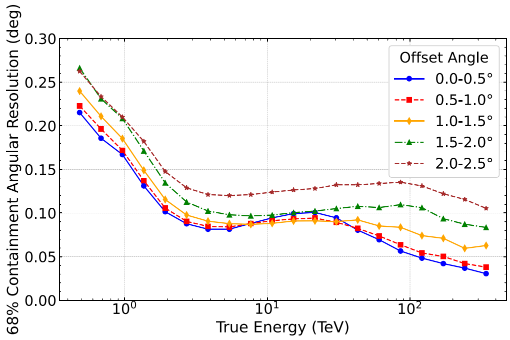

Fig. 5. (color online) Angular resolution for different offset angles (zenith angle: 60°).

particularly suitable for observing extended sources. Additionally, the smaller images allow our cameras to have a smaller field of view without compromising performance. The off-axis performance was evaluated using Monte Carlo diffuse gamma events. In Fig. 5, we show the angular resolution at different offsets for LZA. It can be observed that when the offset is less than 2°, we can still achieve a reasonable angular resolution (better than 0.1°).

C. Overall performance and discussion

As mentioned above, energy reconstruction was performed using a RandomForestRegressor model trained on simulated diffuse γ-ray events; the results at LZA are shown in Fig. 6. In most energy ranges, the energy resolution is better than 10%, allowing for accurate spectral measurements. We also calculated the differential sensitivity for 50 h of observation. The following three conditions were considered: (1) significance greater than 5 (calculated using Eq. (17) from Ref. [30] and assumed $\alpha = 0.2$); (2) detection of at least 10 photons; and (3) $N_\gamma/N_{\rm background} > 5\%$, given the systematic uncertainty of background estimation. In each energy bin, we optimized the theta and particle separation cuts to maximize the differential sensitivity. The on-axis differential sensitivity is shown in Fig. 7. Owing to the improved angular resolution at LZA and the nearly tripled effective area, we achieved excellent sensitivity. Compared to the sensitivity of existing IACTs at 20° zenith angle, the eight-telescope subarray of LACT at LZA demonstrates approximately ten times better sensitivity above 30 TeV, approaching that of CTA-South. This exceptional sensitivity allows LACT to achieve significant results in a relatively short observation time.

It is important to note that because the layout of the eight telescopes is not perfectly symmetrical, the performance we obtained is likely to depend on the azimuth angle. This dependency could be more pronounced at LZA, requiring further investigation to understand its impact on the overall performance.

Moreover, in the LZA observation mode, LHAASO

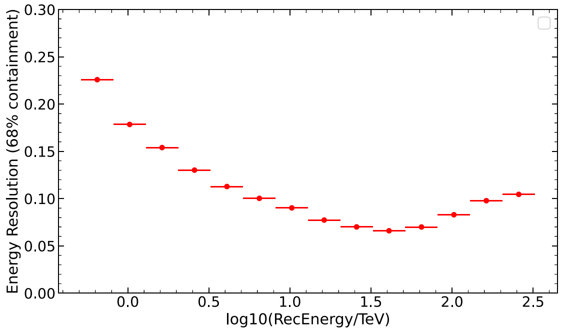

Fig. 6. (color online) Energy resolution for eight telescopes (zenith angle: 60°).

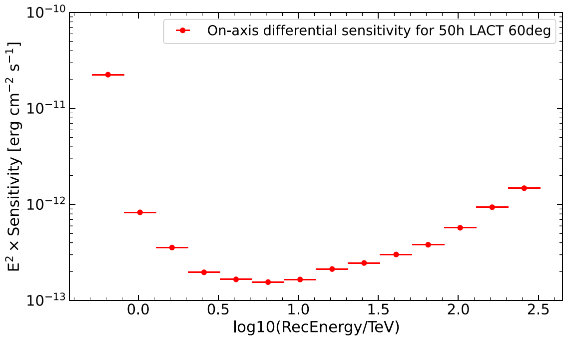

Fig. 7. (color online) Differential sensitivity for eight telescopes (zenith angle: 60°).

can still provide valuable information. LHAASO-KM2A consists of two main components: the Electromagnetic particle Detector (ED) and the Muon Detector (MD). The ED is designed to measure the density and arrival time of electromagnetic particles from extensive air showers [31], while the MD plays a crucial role in discriminating cosmic ray background [32], thus improving the detection sensitivity for gamma rays. Owing to the absorption of electromagnetic particles at LZA, it is challenging for the ED of KM2A to function effectively. However, the MD remains operational under these conditions. Given that LACT can provide excellent angular resolution and core position accuracy for KM2A, the MD can still play a significant role in particle separation at LZA. Ongoing research is focused on integrating MD data, which will further enhance the particle separation capabilities of LACT.

As mentioned in Ref. [33], for LZA observation, the accumulation of more clouds and dust makes atmospheric monitoring even more crucial. At the LHAASO site, using lasers to monitor the atmosphere up to approximately 50 km has proven to be highly effective [34]. Additional monitoring equipment will also be installed to assist LACT with calibration.

IV. SMALL ZENITH ANGLE PERFORMANCE

Traditional IACTs typically observe at zenith angles below 50°. Compared to the LZA mode, small zenith angles allow for a lower energy threshold. Therefore, in addition to ensuring ultra-high energy observations at LZA, LACT also aims to achieve synergy with WCDA, particularly in time-domain γ-ray astronomy and extragalactic astronomy, for example, in detection of GRBs [35] and Blazars. In contrast to LZA observations, small zenith angle observations benefit from a relatively close separation between telescopes to achieve optimal performance. Based on the optimization for LZA, we divided the 32 telescopes into 8 well-separated cells, with each cell containing four closely spaced telescopes. In subsequent analyses, we set the distance between different cells to 400 m.

A. Optimization of individual CELL

First, we consider the performance of a single CELL. Given the large distances between CELLs, the performance of the array at low energies is similar to the arithmetic summation of eight individual CELLs. A H.E.S.S like squared CELL is considered. We investigated the performance with side lengths of 100, 120, 140, 160, and 180 m. The angular resolution and differential detection rate are shown in Figs. 8 and 9. The differential detection rate $R(E)$was computed using the formula $R(E) = \Phi(E)\times A(E)$, where $\Phi(E)$ represents the primary γ-ray differential energy spectrum of the Crab Nebula [36], and $A(E)$ is the collection area. From the differential detection rate, we can determine the energy threshold, which is typically defined as the energy corresponding to the maximum differential detection rate. Interestingly, Fig. 9 reveals that closer distances between telescopes do not result in lower energy thresholds. For CELLs with different side lengths, the corresponding energy thresholds all converged around 200 GeV. To understand this phenomenon, we examined the lateral photon distribution for different energies at the altitude of LHAASO, that is, 4 410 m. The results are shown in Fig. 10.

At the high altitude of LHAASO, the lateral distribution of photons is steeper compared to lower altitudes. Therefore, for several TeVs γ-ray showers, there is no light pool [37] present. As the energy decreases, the lateral distribution becomes flatter. Only below 200 GeV will a γ-ray shower produce a light pool with a radius of approximately 120 m. Within the confines of this light pool, the photon density remains essentially constant. Therefore, closer distances cannot effectively increase the collection area below 200 GeV, resulting in a nearly universal energy threshold.

Additionally, for energies above 800 GeV, CELLs with larger side lengths exhibit significantly higher angular resolution. Figure 11 shows the relationship between *MISS* and impact parameters at different energies, indicating that the distance corresponding to the minimum *MISS* is around 120 m for most energy ranges. As the impact parameter increases, *MISS* initially decreases and

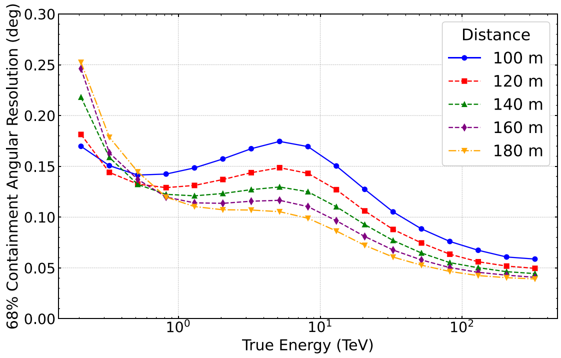

Fig. 8. (color online) Angular resolution for CELLs with different side lengths (zenith angle: 20°).

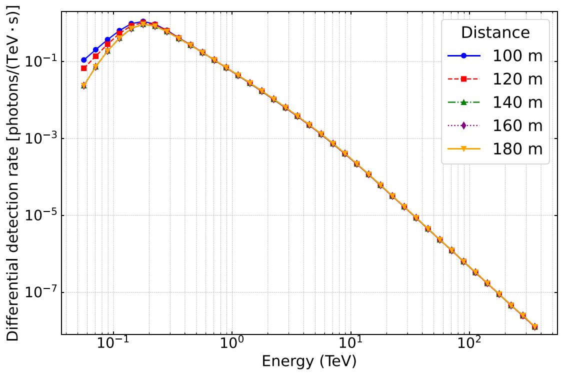

Fig. 9. (color online) Differential detection rate for CELLs with different side lengths (Zenith Angle 20°).

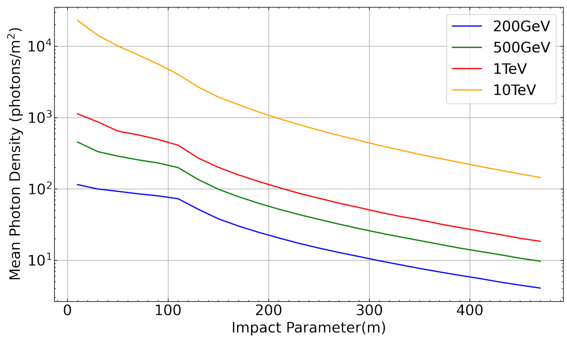

Fig. 10. (color online) Lateral distributions for 200 GeV, 500 GeV, 1 TeV, and 10 TeV photons obtained from CORSIKA simulations at an altitude of 4 400 m above sea level, without accounting for atmospheric absorption.

then increases. This is because, at smaller impact parameters, geometric factors cause the image in the telescope to become more elongated, resulting in better accuracy. However, as the impact parameter continues to grow, the image moves closer to the edge of the camera, and leakage degrades the imaging quality. For high-energy events, more events will fall outside the CELL. Therefore, larger side lengths allow more telescopes to be positioned where reconstruction accuracy is higher, resulting in better angular resolution. This can be verified in

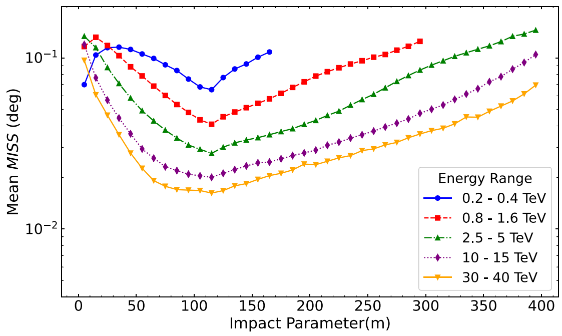

Fig. 11. (color online) Mean *MISS* versus impact parameter at different energies for a 20° zenith angle.

Fig. 12, which shows the distribution of impact parameters for the nearest and second nearest telescopes for 2.5 to 5 TeV γ-ray events, comparing side lengths of 100 and 180 m. We can see that at 180 m, the nearest telescopes are more frequently positioned between 70 and 200 m, a range that allows for optimal reconstruction accuracy.

B. Comparison of all telescopes

Besides individual CELLs, we investigated the performance of 32 telescopes for various CELL side lengths. Figure 13 shows the layout for a side length of 160 m.

Compared to individual CELLs, the performance differences across various CELL side lengths become much smaller when considering all 32 telescopes.

This is because, in the full array mode, when an event moves away from one CELL, it becomes closer to adjacent CELLs. As a result, the performance differences between individual CELLs become less significant. In Fig. 14, we compare the angular resolution between a single CELL and the full array. For energies below 1 TeV, the angular resolutions of both the CELL and the array are nearly identical, indicating that low-energy events are mostly contained within a single CELL. As the energy increases, "cross-talk" between different CELLs leads to a significant improvement in the performance of the full array compared to an individual CELL. However, above 100 TeV, the difference between the CELL and the full array decreases, suggesting that, owing to leakage, the multiplicity of high-energy events is reduced.

C. Overall performance

Based on the above analysis, we can conclude that when considering the performance of all 32 telescopes in the LACT array, the differences in performance between cells of varying side lengths are relatively small. However, for individual cells, larger side lengths provide higher performance, particularly in terms of angular resolution for higher energy events. To maintain a balance between overall array performance and flexibility of individual cell observations, the optimal side length between cells should range from 140 to 180 m. Excessively large

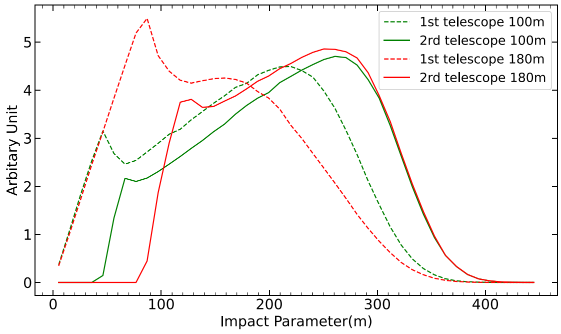

Fig. 12. (color online) Distribution of impact parameters for the nearest and second nearest telescopes for a range of energies from 2.5 TeV to 5 TeV, comparing CELLs with side lengths of 180 and 100 m.

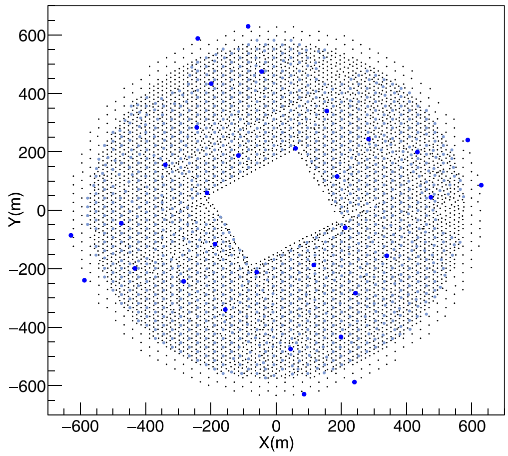

Fig. 13. (color online) Layout of LACT and LHAASO. The side length of CELL was set to be 160 m. The small black dots represent the electromagnetic particle detectors (EDs) of LHAASO-KM2A, the small light blue circles represent the muon detectors (MDs), and the blue circles represent the LACT telescopes.

side lengths would result in telescopes within different cells being too close to each other, potentially negatively impacting the performance of the entire array. In Figs. 15 and 16, we present the energy resolution and differential sensitivity of the entire array with a side length of 140 m. The energy resolution of the full array ranges from approximately 10% to 20%, reaching its best value of approximately 9% near 5 TeV. Compared to that at LZA, the energy resolution at high energies is significantly worse owing to increased image leakage and reduced multiplicity. The differential sensitivity of the full LACT array shows a remarkable improvement over existing IACTs. At energies of a few hundred GeV, the sensitivity of the full LACT array is approximately twice as good as that of HESS or VERITAS. As the energy increases, this gain becomes even more pronounced. Above a few TeV, LACT is expected to become the most sensitive IACT in the Northern Hemisphere.

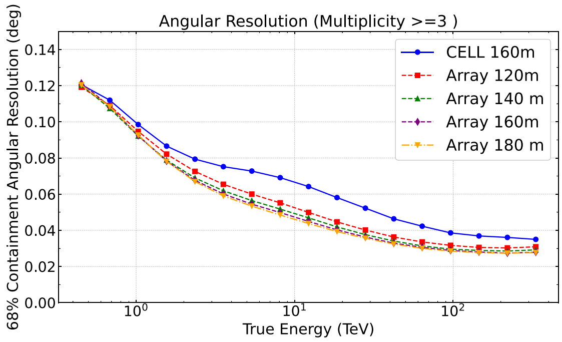

Fig. 14. (color online) Angular resolution for different configurations: "CELL" represents four square-like telescopes, while "Array" represents all 32 telescopes. The plot compares the angular resolution for various array side lengths, including the angular resolution for a single CELL with a side length of 160 m. Here, we apply a relatively strict cutoff, requiring the multiplicity to be greater than three.

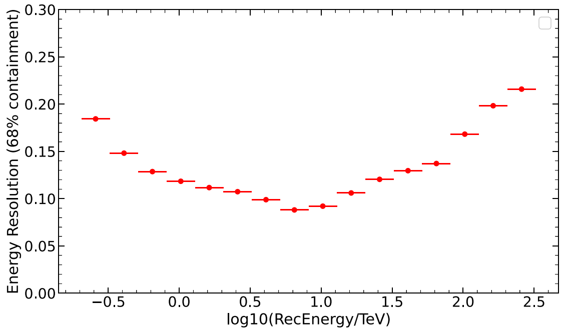

Fig. 15. (color online) Energy resolution for 32 telescopes. The side length is set to 140 m (zenith angle: 20°).

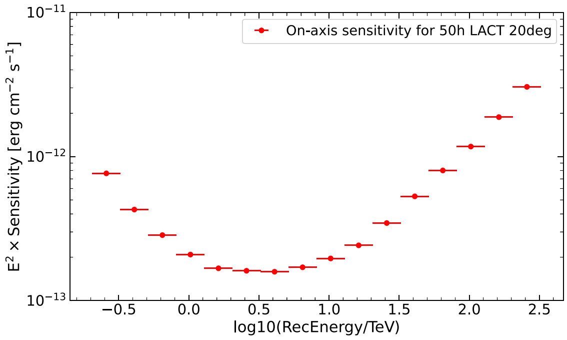

Fig. 16. (color online) Differential sensitivity for 32 telescopes. The side length is set to 140 m (zenith angle: 20°).

V. CONCLUSIONS

The primary scientific objective of LACT is to perform in synergy with LHAASO, which presents two key aspects. The first is to work in synergy with LHAASO-KM2A for deep observations of ultra-high-energy γ-ray sources and to study their morphology in detail, thereby confirming the existence of PeVatrons. To achieve this, we use the LZA observation mode to enhance our effective area. In this study, we examined the performance of eight telescopes at a 60° zenith angle. Compared to a 20° zenith angle, both the effective area and angular resolution show significant improvement. This eight-telescope subarray can achieve sensitivity approaching that of CTA-South and can effectively work in synergy with LHAASO-KM2A. Additionally, the four eight-telescope subarrays of LACT allow simultaneous observations of different sources, significantly increasing the observation time for each source. This capability enables deep observations of key targets, providing the potential for detailed spectral and morphological studies of PeVatron candidates. In Fig. 17, we compare the differential sensitivity of LACT after 500 h of observation in two modes with that of LHAASO after one year. In both modes, LACT demonstrates sensitivity comparable to that of LHAASO. Notably, in the LZA mode, LACT shows superior differential sensitivity below 100 TeV. This positions LACT as a valuable complement to LHAASO, with the potential to significantly advance our understanding of high-energy astrophysical phenomena. In Table 2, we present the observation times for several important sources from October 1, 2024, to April 1, 2025, which is considered an optimal observation period for LACT. The table includes observations at zenith angles below 50° and between 50°–70°. From this table, it is clear that substantial observation times can be achieved at large zenith angles for these sources. Notably, sources such as the Galactic Center can only be effectively observed at LZA, underscoring the importance of LZA observations in expanding the sky coverage and scientific capabilities of LACT.

The second objective is to achieve a lower energy threshold at small zenith angles and collaborate with LHAASO-WCDA on various scientific topics. With the construction of next-generation Cherenkov telescopes like CTA and ASTRI, there is an increasing demand for the ability to rapidly follow up on transient phenomena and continuously monitor them [38]. The energy threshold of the entire LACT array is approximately 200 GeV at a 20° zenith angle, allowing for a well-connected observed energy spectrum with Fermi-LAT and excellent synergy with LHAASO-WCDA. This capability is crucial for studying transient events such as gamma-ray bursts (GRBs) and active galactic nuclei (AGNs).

In subsequent studies, we will further investigate the synergy between LHAASO and LACT. This synergy extends beyond the scientific cases mentioned earlier, encompassing experiments such as joint event reconstructions using different detectors from LHAASO and LACT. As highlighted in previous research [28], during long-term observations of extended sources, particle discrimination is crucial owing to the background count being much higher than that of point sources. The inclusion of the muon detector of KM2A will significantly enhance the performance of LACT in these long-term observations. Additionally, it is important to note that the simulation parameters currently used do not perfectly align with those of the actual LACT telescope. The first LACT prototype is scheduled for completion by the end of 2024. The observational data from this prototype will improve our understanding of the simulations, allowing future Monte Carlo simulations to validate our analysis methods and produce more realistic performance curves.

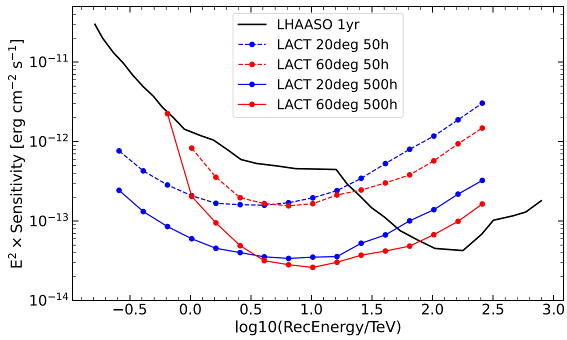

Fig. 17. (color online) A comparison of LACT sensitivity for 500 and 50 h of exposure in two observation modes, alongside LHAASO sensitivity after one year. In the 20° mode, all 32 LACT telescopes are utilized, while in the 60° mode, an 8-telescope subarray is employed. The LHAASO sensitivity data points are extracted from [7].

Table 2. Observation times for specific sources by LACT between October 1, 2024, and April 1, 2025, categorized by zenith angles below 50° and between 50°–70°. This calculation assumes ideal conditions and does not account for weather factors.

Source	RA	DEC	0–50°	50°–70°
SS433	19h10m37s	+05d02m13s	75h	152h
J1908+0621	19h08m12s	+06d21m0s	76.25h	154.75h
Galactic center	17h45m39.6s	-29d0m22s	0h	37h
J1825-134	18h25m49s	-13d46m35s	2.5h	99h
J2226+6057	22h27m0s	+60d57m	386h	371h
cygnus	20h31m33s	+41d34m38s	217h	233h

References

[1] F. Krennrich, C. W. Akerlof, J. H. Buckley *et al*., Astropart. Phys. **8**(4), 213 (1998)

[2] M. Amenomori, Z. Cao, L. K. Ding *et al*., Phys. Rev. Lett. **69**(17), 2468 (1992)

[3] C. Bacci, K. Z. Bao, F. Barone *et al*., Astropart. Phys. **17**(2), 151 (2002)

[4] F. Aharonian, A. G. Akhperjanian, A. R. Bazer-Bachi *et al.*, Astron. Astrophys. **457**(3), 899 (2006)
[5] E. Aliu, T. Arlen, T. Aune, *et al.*, Science **334**(6052), 69 (2011)
[6] J. Aleksić, E. A. Alvarez, L. A. Antonelli *et al.*, Astropart. Phys. **35**(7), 435 (2012)
[7] Z. Cao, D. della Volpe, S. M. Liu *et al*. *The large high altitude air shower observatory (lhaaso) science book*(2021 Ed.)., arXiv: 1905.02773
[8] Z. Cao, F. A. Aharonian, Q. An *et al.*, Nature **594**(7861), 33 (2021)
[9] Z. Cao, F. Aharonian, Q. An *et al.*, Astrophys. J. Suppl. S. **271**(1), 25 (2024)
[10] Z. Cao, S. Z. Chen, R. Y. Liu *et al.*, Annu. Rev. Nucl. Part. Sci. **73**, 341 (2023)
[11] B. S. Acharya, M. Actis, T. Aghajani *et al.*, Astropart. phys. **43**, 3 (2013)
[12] S. Vercellone, C. Bigongiari, A. Burtovoi *et al.*, J. High Energy Astrophys. **35**, 1 (2022)
[13] S. S. Zhang. Large Array of imaging atmospheric Cherenkov Telescopes (LACT): status and future plans. In *Proceedings of 38th International Cosmic Ray Conference — PoS(ICRC2023)*, volume 444, page 808, 2024.
[14] A. V. Plyasheshnikov, F. A. Aharonian, and H. J. Völk, J. Phys. G: Nucl. Part. **26**(2), 183 (2000)
[15] G. P. Rowell, V. Stamatescu, R. W. Clay *et al.*, Nucl. Instrum. Meth. A **588**(1-2), 48 (2008)
[16] A. Nada, A. Ramos, Eur. Phys. J. C **81**, 1 (2021)
[17] S. C. Hu, G. M. Xiang, M. Zha *et al.*, PoS **ICRC2023**(2), 655 (2023)
[18] D. Heck, J. Knapp, J. N. Capdevielle *et al*. Corsika: A monte carlo code to simulate extensive air showers. 1998.
[19] K. Bernlöhr, Astropart. Phys. **30**(3), 149 (2008)
[20] K. Bernlöhr, A. Barnacka, Y. Becherini *et al.*, Astropart. Phys. **43**, 171 (2013)
[21] A. Michael Hillas. Cerenkov light images of eas produced by primary gamma. In *19th Intern. Cosmic Ray Conf-Vol. 3*, number OG-9.5-3, 1985.
[22] F. Pedregosa, G. Varoquaux, A. Gramfor *et al.*, J. Mach. Learn. Res. **12**, 2825 (2011)
[23] P. Sommers and J. W. Elbert, J. Phys. G: Nucl. Phys. **13**(4), 553 (1987)
[24] A. Konopelko, F. Aharonian, M. Hemberger *et al.*, J. Phys. G: Nucl. Phys. **25**(9), 1989 (1999)
[25] V. A. Acciari, S. Ansoldi, L. A. Antonelli *et al.*, Astron. Astrophys. **635**, A158 (2020)
[26] C. B. Adams, W. Benbow, A. Brill *et al.*, Astrophys. J. **913**(2), 115 (2021)
[27] C. C. Lu. Improving the hess angular resolution using the disp method, arXiv: 1310.1200
[28] Z. P. Zhang *et al.*, J. High Energy Astrophys. **43**, 280 (2024)
[29] E. Giro, R. Canestrari, G. Siron *et al.*, Astron. Astrophys. **608**, A86 (2017)
[30] T. P. Li and Y. Q. Ma, Astrophys. J. **272**, 317 (1983)
[31] J. Zhao, J. Liu, X. D. Sheng *et al.*, Chin. Phys. C **38**(3), 036002 (2014)
[32] H. Wang, C. Li, G. Xiao *et al.*, Nucl. Instrum. Meth. A **956**, 163416 (2020)
[33] M. Peresano, *et al* (MAGIC Collaboration), Nuovo Cimento C Geophysics Space Physics C **41**(3), 107 (2018)
[34] Q. N. Sun, F. R. Zhu, Y. Zhang *et al.*, Nucl. Instrum. Meth. A **1057**, 168759 (2023)
[35] LHAASO Collaboration, Sci. Adv. **9**(46), eadj2778 (2023)
[36] F. Aharonian, A. Akhperjanian, M. Beilicke *et al.*, Astrophys. J. **614**(2), 897 (2004)
[37] H. J. Völk and Konrad Bernlöhr, Exp. Astron. **25**, 173 (2009)
[38] S. Lee, S. Einecke, G. Rowell *et al.*, Publications of the Astronomical Society of Australia **39**, e041 (2022)